PERGAMON

International Journal of Heat and Mass Transfer 42 (1999) 2345–2355

International Journal of HEAT and MASS TRANSFER

Natural convection in rectangular enclosures heated from one side and cooled from the ceiling

Orhan Aydin*, Ahmet Ünal, Teoman Ayhan

Department of Mechanical Engineering, Karadeniz Technical University, 61080, Trabzon, Turkey

Received 24 October 1997; in final form 14 September 1998

Abstract

Steady natural convection of air in a two-dimensional enclosure isothermally heated from one side and cooled from the ceiling is analyzed numerically using a stream function–vorticity formulation. Based on numerical predictions, the effects of Rayleigh number and aspect ratio on flow pattern and energy transport are investigated for Rayleigh numbers ranging from 10^3 to 10^7, and for five different aspect ratios of 0.25, 0.50, 1.0, 2.0 and 4.0. The effect of Rayleigh number on heat transfer is found to be more significant when the enclosure is shallow ($a_r > 1$) and the influence of aspect ratio is stronger when the enclosure is tall and the Rayleigh number is high.

Nomenclature

a_r aspect ratio, dimensionless
g gravitational acceleration [m/s^2]
Gr Grashof number, dimensionless
H height of the enclosure [m]
L length of the enclosure [m]
n coordinate in normal direction
Nu Nusselt number, dimensionless
Pr Prandtl number, dimensionless
Ra Rayleigh number, dimensionless
T temperature [K]
t time [s]
u velocity component in x-direction [m/s]
U nondimensional velocity component in x-direction
v velocity component in y-direction [m/s]
V nondimensional velocity component in y-direction
x, y coordinates defined in Fig. 1
X, Y nondimensional coordinates.

Greek symbols

α thermal diffusivity [m^2/s]
β thermal expansion coefficient [1/K]
ζ vorticity [1/s]
θ nondimensional temperature
ξ nondimensional vorticity
τ nondimensional time
ψ stream function [m^2/s]
Ψ nondimensional stream function
Φ generalized nondimensional variable.

Subscripts

C cold wall
H hot wall
i, j coordinate indices
wall at wall
x in x-direction
y in y-direction.

1. Introduction

In many engineering applications and naturally occurring processes, natural convection plays an important role as a dominating mechanism. Besides its importance in such processes, due to the coupling of fluid flow and energy transport, the phenomenon of natural convection remains an interesting field of investigation.

There are numerous studies in the literature regarding natural convection in enclosures, a considerable amount of which is given in a review by Ostrach [1]. Most of the previous studies on natural convection in enclosures are related to either side heating or bottom heating [2–8].

Although many different boundary conditions are

* Corresponding author. Tel.: +462 3253223; fax: +462 3255526; e-mail: aydin@ovms02.ktu.edu.tr

0017–9310/99/$ - see front matter
PII: S0017–9310(98)00319–6

present in practice, there are a limited number of studies available in the literature dealing with more complex boundary conditions. Hasnaoui et al. [9] investigated natural convection in an enclosure with localized heating from below. Ganzarolli and Milanez [10] conducted a numerical study for steady natural convection in an enclosure heated from below and symmetrically cooled from the sides. Valencia and Frederick [11] numerically investigated natural convection of air in square cavities with half-active and half-insulated vertical walls for Rayleigh numbers from 10^3 to 10^7. Chinnokotla et al. [12] performed a parametric study on buoyancy-induced flow and heat transfer from L-shaped corners with asymmetrically heated surfaces. Selamet and Arpaci [13] studied natural convection in a vertical slot with narrow upper section and investigated the effect of a sudden-change in hot wall temperature on flow and energy transport. Chu et al. [14] conducted an experimental and numerical study to investigate the effects of heater size, heater location, aspect ratio, and boundary conditions on two-dimensional laminar natural convection in rectangular enclosures. November and Nansteel [15] studied the natural convective flow in a square enclosure with a cooled vertical wall and a heated floor. Poulikakos [16] reported numerical results for natural convection in an enclosure heated and cooled along a single wall. In their numerical study, Aydin et al. [17] considered the case of a square enclosure heated from one side and cooled from above, and investigated the influence of Prandtl number on flow field and energy transport.

In the present study, natural convection in a rectangular enclosure heated from one side and cooled from the ceiling is analyzed numerically. Both the hot wall and cold ceiling temperatures are assumed to be uniform. This type of boundary conditions has a practical importance especially in cooled ceiling applications. The main objective of this study is to determine the effect of aspect ratio and Rayleigh number on flow pattern and heat transfer in the enclosure.

2. Analysis

The geometry and coordinate system of the problem under consideration is depicted in Fig. 1. The size of the enclosure in z-direction is assumed to be infinitely long. The enclosure is heated from one side and cooled from the ceiling while the other side wall and the floor are perfectly insulated. The hot wall and cold ceiling are considered to be isothermal at T_H and T_C, respectively and the other side wall and floor adiabatic.

2.1. Mathematical formulation

The nondimensional set of the governing equations (stream function, vorticity and energy equations) for a two-dimensional, incompressible laminar flow with constant fluid properties are given as [17]

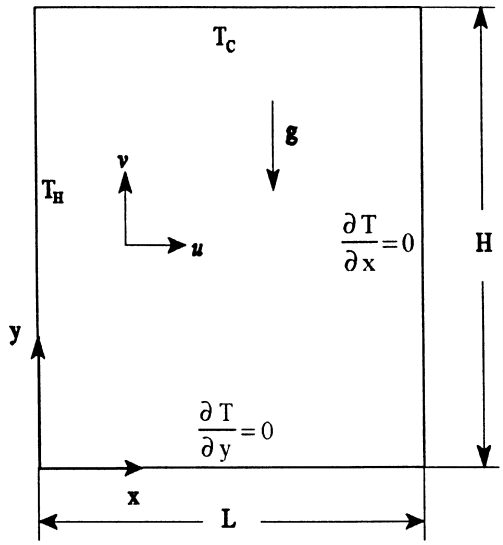

Fig. 1. Geometry and coordinate system.

$$\frac{\partial^2\Psi}{\partial X^2}+\frac{\partial^2\Psi}{\partial Y^2}=-\xi \tag{1}$$

$$\frac{\partial\xi}{\partial\tau}+U\frac{\partial\xi}{\partial X}+V\frac{\partial\xi}{\partial Y}=Pr\left(\frac{\partial\xi^2}{\partial X^2}+\frac{\partial\xi^2}{\partial Y^2}\right)+RaPr\frac{\partial\theta}{\partial X} \tag{2}$$

$$\frac{\partial\theta}{\partial\tau}+U\frac{\partial\theta}{\partial X}+V\frac{\partial\theta}{\partial Y}=\frac{\partial^2\theta}{\partial X^2}+\frac{\partial^2\theta}{\partial Y^2} \tag{3}$$

where the nondimensional parameters including stream function and vorticity are defined in the following forms:

$$X=\frac{x}{H}\quad Y=\frac{y}{H}\quad \theta=\frac{T-T_C}{T_H-T_C}$$

$$\tau=\frac{\alpha t}{H^2}\quad U=\frac{u}{\alpha/H}\quad V=\frac{v}{\alpha/H} \tag{4}$$

$$U=\frac{\partial\Psi}{\partial Y}\quad V=-\frac{\partial\Psi}{\partial X}\quad \xi=\frac{\partial V}{\partial X}-\frac{\partial U}{\partial Y} \tag{5}$$

Appearing in eqn (3), $Pr=v/\alpha$ is the Prandtl number and $Ra=g\beta H^3(T_H-T_C)/v\alpha$ is the Rayleigh number.

2.2. Boundary conditions

Through the introduction of the nondimensional parameters into the physical boundary conditions illustrated in Fig. 1, the following nondimensional boundary conditions are obtained [17]:

$$\theta=1\quad U=0\quad V=0\quad \text{at}\quad X=0\quad \text{and}\quad 0<Y<1 \tag{6}$$

$$\frac{\partial\theta}{\partial X}=0 \quad U=0 \quad V=0 \quad \text{at} \quad X=a_r \quad \text{and} \quad 0<Y<1 \tag{7}$$

$$\frac{\partial\theta}{\partial Y}=0 \quad U=0 \quad V=0 \quad \text{at} \quad Y=0 \quad \text{and} \quad 0<X<a_r \tag{8}$$

$$\theta=0 \quad U=0 \quad V=0 \quad \text{at} \quad Y=1 \quad \text{and} \quad 0<X<a_r \tag{9}$$

where $a_r = L/H$ is the aspect ratio of the enclosure.

For stream function, the boundary condition for entire surface of the enclosure is taken to be

$$\Psi=0 \tag{10}$$

which implies that there is no mass transfer through the walls of the enclosure and that the boundaries themselves form one of the streamlines [2].

In general, the value of the vorticity on a solid boundary is deduced from Taylor series expansion of the stream function Ψ around the solid point [18] and can be expressed mathematically as

$$\xi_{\text{wall}} = -\frac{\partial^2\Psi}{\partial n^2} \tag{11}$$

where ξ_{wall} is the value of the vorticity at wall and n is the outward drawn normal of the surface. In numerical calculations, the values of vorticity at corners are taken as averages of the values of vorticity at two neighbouring nodes.

2.3. Average Nusselt numbers for hot and cold walls

The average Nusselt numbers, $\overline{Nu_y}$ for heated vertical wall and $\overline{Nu_x}$ for cooled ceiling are given by

$$\overline{Nu_y} = \int_0^1 Nu(Y)\,\mathrm{d}Y \tag{12}$$

$$\overline{Nu_x} = \frac{1}{a_r}\int_0^{a_r} Nu(X)\,\mathrm{d}X \tag{13}$$

where $Nu(Y)$ and $Nu(X)$ are local Nusselt numbers for heated side wall and cooled ceiling, respectively and are given by

$$Nu(Y) = \left[-\frac{\partial\theta}{\partial X}\right]_{X=0} \tag{14}$$

$$Nu(X) = \left[-\frac{\partial\theta}{\partial Y}\right]_{Y=1} \tag{15}$$

2.4. Numerical procedure

The governing equations along with the boundary conditions are solved numerically, employing finite-difference techniques. The vorticity transport and energy equations are solved using the Alternating Direction Implicit method of Peaceman and Rachford [19], and the stream function equation is solved by SOR (successive over-relaxation) method [20]. The over-relaxation parameter is chosen to be 1.8 for stream function solutions. In order to avoid divergence in the solution of vorticity equations an under-relaxation parameter of 0.5 is employed. The buoyancy and diffusive terms are discretized by using central differencing while the use of upwind differencing is preferred for convective terms for numerical stability. Starting from arbitrarily specified initial values of variables, the discretized transient equations are then solved by marching in time until an asymptotic steady-state solution is reached. Convergence of iteration for stream function solution is obtained at each time step. The following criterion is employed to check for steady-state solution

$$\sum_{i,j}|\Phi_{i,j}^{n+1}-\Phi_{i,j}^{n}| \leqslant \varepsilon \tag{16}$$

where Φ stands for Ψ, ξ or θ; n refers to time and i and j refer to space coordinates. The value of ε is chosen as 10^{-5}. The time step used in the computations is varied between 0.00001 and 0.004, depending on Rayleigh number and mesh size. All the computations are carried out on a Vax 6000-520 mainframe computer.

A grid independence study is conducted using four different grid sizes of 21×21, 31×31, 41×41, and 61×61 for $a_r = 1.00$ and it is observed that a further refinement of grids from 41×41 to 61×61 does not have a significant effect on the results in terms of average Nusselt number and the maximum value of the stream function. Based on this observation, a uniform grid of 41×41 points is used for all of the calculations for $a_r = 1.00$. Similar grid dependency studies are carried out for the other aspect ratios and an optimum grid size is obtained for each aspect ratio. In addition, the grid size dependent effect of the discontinuity in temperature at the intersection of the hot and cold walls on the local Nusselt number is taken care of by using a well defined temperature profile in this corner region. Although the temperature discontinuity at this corner has no influence on the numerical calculation of the interior temperatures and the flow field, due to the non-integrable singularity of heat flux at this point, it is necessary to make some considerations about this singular point [11]. The simplest way of handling this problem is assuming the average temperature of the two walls at the corner and keeping the adjacent nodes with the respective wall temperatures. Ganzorolli and Milanez [11] assumed a linear temperature profile between the corner node and the next adjacent node and performed some tests to determine the grid dependence of average Nusselt number. Even though their tests showed that the grid dependence of the average Nusselt number is important for very coarse meshes only, the grid dependence of the local Nusselt number at this corner is very significant. The local Nusselt number at this corner

becomes larger and larger as the grid is refined. In fact, this is not very meaningful as far as the real physical systems are concerned. When the two walls at different temperatures come into a perfect physical contact, the interface will assume a thermal equilibrium at an intermediate temperature and, depending on the thermal conductivity of the respective wall material, there will be a temperature distribution in the wall in some neighbourhood of the corner. Based on this argument, we assumed that the corner node is at the average temperature and we adopted linear temperature distributions in very small sections (the sizes of which are independent of the grid size) of both walls in the neighbourhood of the top left corner.

In order to test the computer code developed in this study, the problem of buoyancy-driven flow in a square cavity that has differentially heated vertical walls and adiabatic upper and bottom walls is studied. A very good agreement is obtained between the test problem solution and the bench mark solution of de Vahl Davis [21]. The temperature distribution data and the average Nusselt numbers for very low Rayleigh numbers are also compared with pure conduction solution obtained through the separation of variables and a perfect agreement is observed.

3. Results and discussion

Computations are carried out for air as working fluid with a Prandtl number of 0.71. The effect of aspect ratio a_r is studied by considering five different values: 0.25, 0.5, 1.0, 2.0, and 4.0. It is worth to note that in this study the aspect ratio $a_r = L/H$ is equal to the ratio of cold wall

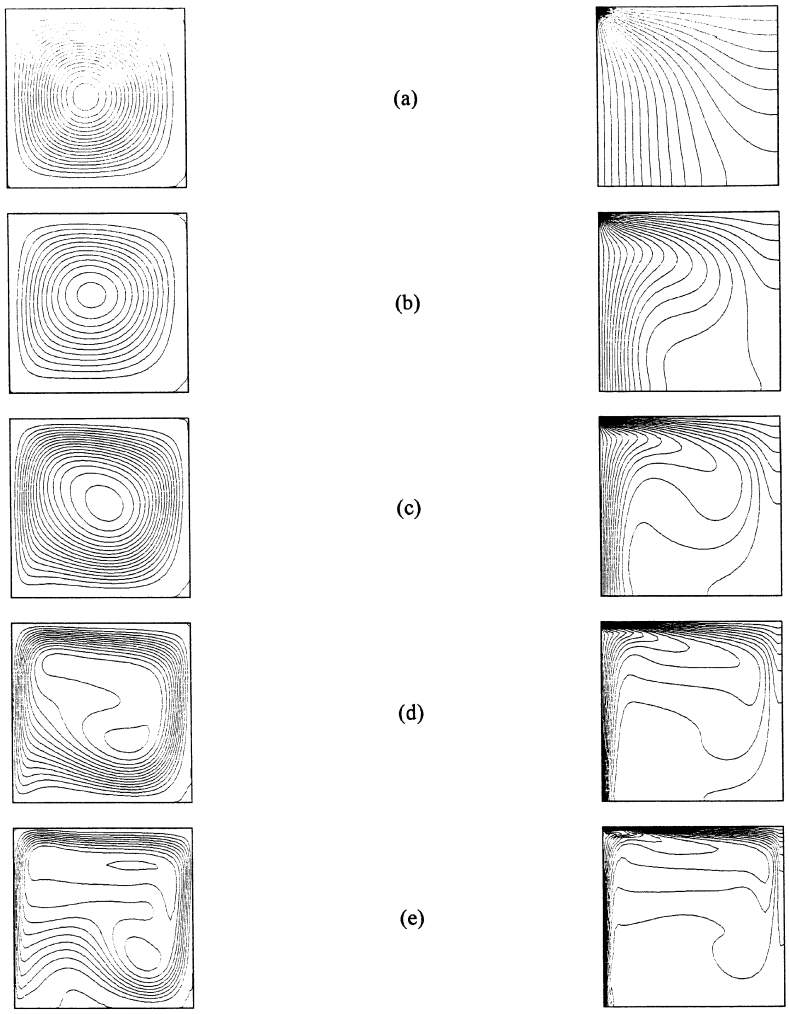

Fig. 2. Streamlines and isotherms for $a_r = 1.0$: (a) $Ra = 10^3$; (b) $Ra = 10^4$; (c) $Ra = 10^5$; (d) $Ra = 10^6$; (e) $Ra = 10^7$.

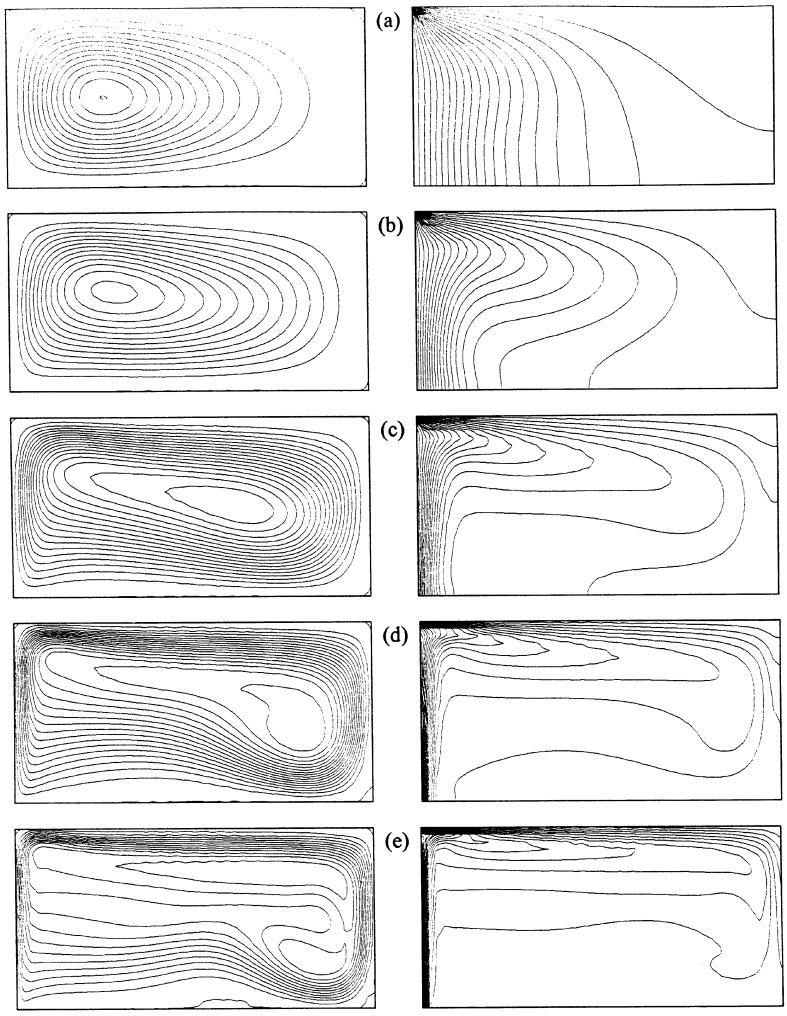

Fig. 3. Streamlines and isotherms for $a_r = 2.0$: (a) $Ra = 10^3$; (b) $Ra = 10^4$; (c) $Ra = 10^5$; (d) $Ra = 10^6$; (e) $Ra = 10^7$.

length L_C to hot wall length L_H. The effect of Rayleigh number is investigated in the range of $10^3 \leqslant Ra \leqslant 10^7$. The results are presented in Figs. 2–6 in the form of streamlines and isotherms. In the figures, isotherms represent the lines with equal intervals between zero (at cold wall) and unity (at hot wall), and the streamlines represent the lines having the values between Ψ_{min} and Ψ_{max}.

3.1. Square enclosure

Figure 2 shows the streamlines and isotherms for square enclosure ($a_r = 1$) for various Rayleigh numbers. At $Ra = 10^3$, streamlines form a nearly centrally located single cell and corresponding isotherms exhibit the characteristics of pure conduction forming a diagonally symmetric structure as illustrated by Fig. 2(a). The ascending warmer fluid, which is lifted along the hot wall by a weak clockwise recirculation, is rapidly cooled in the vicinity of cold ceiling by descending colder fluid layer. The interaction of warmer and colder fluid streams results in spreading of isotherms in upper right quadrant of the enclosure and compression in the lower left quadrant. As the Rayleigh number increases, the center of the single cell moves toward lower right corner of the enclosure. As a consequence of increasing convective motion with increasing Rayleigh number, temperature gradients near the heated vertical wall and cooled ceiling become more severe and colder fluid tends to occupy the lower part of the enclosure (Fig. 2(b)). At $Ra = 10^5$, in Fig. 2(c), a thermal boundary layer formation is observed adjacent to the heated and cooled walls. With further increase in Rayleigh number to 10^6 and 10^7, the boundary layers become more distinguished (Fig. 2(d) and (e)).

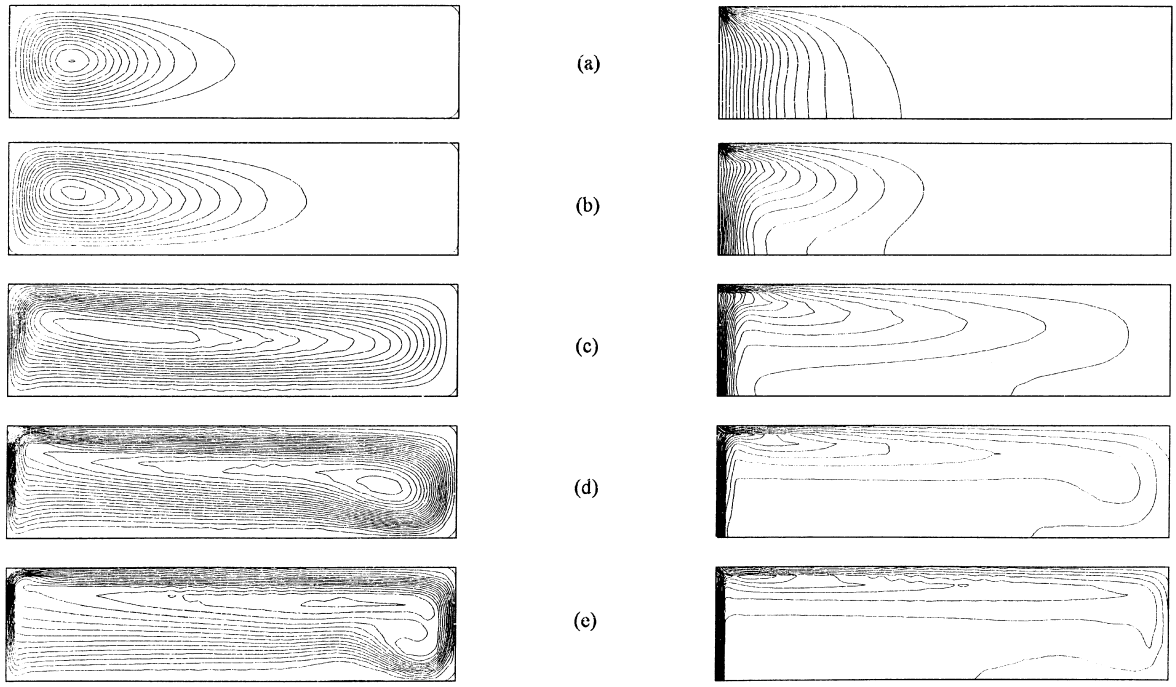

Fig. 4. Streamlines and isotherms for $a_r = 4.0$: (a) $Ra = 10^3$; (b) $Ra = 10^4$; (c) $Ra = 10^5$; (d) $Ra = 10^6$; (e) $Ra = 10^7$.

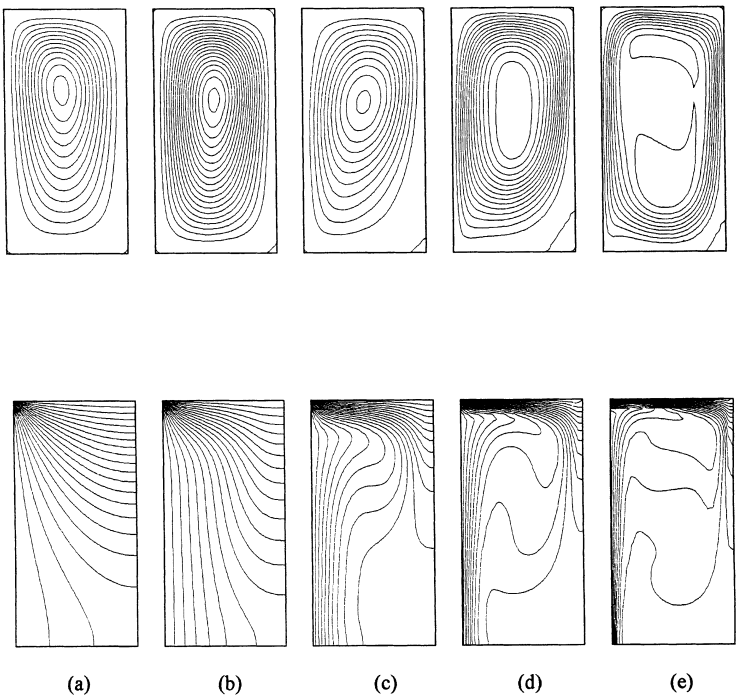

Fig. 5. Streamlines and isotherms for $a_r = 0.5$: (a) $Ra = 10^3$; (b) $Ra = 10^4$; (c) $Ra = 10^5$; (d) $Ra = 10^6$; (e) $Ra = 10^7$.

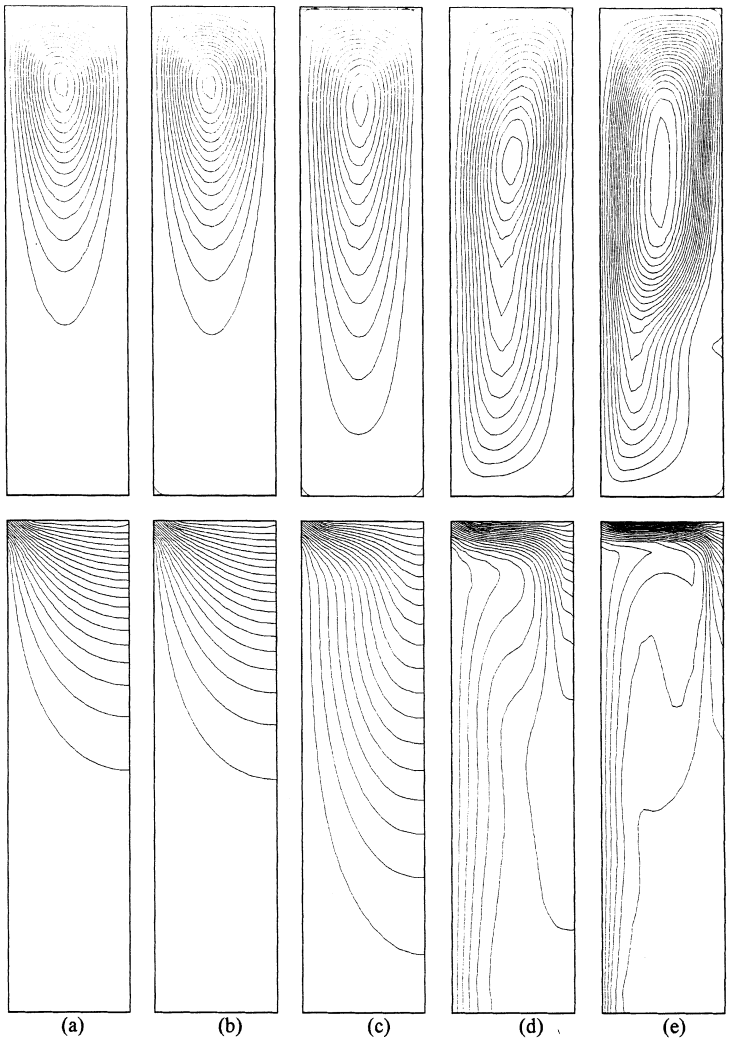

Fig. 6. Streamlines and isotherms for $a_r = 0.25$: (a) $Ra = 10^3$; (b) $Ra = 10^4$; (c) $Ra = 10^5$; (d) $Ra = 10^6$; (e) $Ra = 10^7$.

The asymmetry of the flow is the main difference when compared with flow in a differentially heated enclosure. Temperature gradient on heated vertical wall is maximum at the bottom and decreases from bottom to top. Similar variation of the temperature gradient is observed on a cooled ceiling, the maximum gradient being at the left corner. Therefore, heat flux from hot wall decreases from bottom to top while heat flux to cold ceiling decreases from left to right. For $Ra \geqslant 10^5$ isotherms tend to be increasingly stratified in upper half of the enclosure and the fluid becomes relatively stagnant in the core region.

3.2. Shallow enclosures

The flow pattern and temperature distributions for $a_r = 2$ and $a_r = 4$, representing shallow enclosures, are demonstrated in Figs. 3 and 4, respectively. Similar to the case of square enclosure, a clockwise rotating single cell is observed for both cases at Rayleigh numbers up to 10^6. At $Ra = 10^7$, a second cell is observed at the lower right region. For low Rayleigh numbers the cell, the center of which is located closer to the heated wall, does not occupy the entire enclosure and the isotherms exhibit nearly pure conduction characteristics. As the Rayleigh number increases, the center of the cell moves from left to right along the x-axis and the flow tends to occupy the whole enclosure more uniformly. This phenomenon becomes more pronounced with increasing aspect ratios as it is demonstrated in Fig. 4 for $a_r = 4$. From Fig. 4(a)–(c) we see that, while only one half of the enclosure is occupied at $Ra = 10^3$, the occupied region is extended to 3/4 of the enclosure at $Ra = 10^4$ and to the entire enclosure at $Ra = 10^5$. From the figures it is also observed that

the isotherms for $Ra = 10^3$ become nearly parallel to the heated vertical wall and except the left corner region, the ceiling remains thermally inactive. The fluid serves as an isothermal cold reservoir in this case and heat transfer from hot wall to this reservoir is mainly through heat conduction. As the Rayleigh number increases, the isotherms are distorted along the diagonal of the enclosure due to convection resulting in extension of thermally active zone on the cold ceiling towards insulated vertical wall. However, even at high Rayleigh numbers, thermal boundary layer is established at the vicinity of left corner only.

3.3. Tall enclosures

Figures 5 and 6 show the influence of aspect ratio and Rayleigh number on flow and heat transfer in enclosures having the aspect ratios of $a_r = 0.5$ and $a_r = 0.25$, respectively which are considered to be tall enclosures. At $Ra = 10^3$, the structure of streamlines and isotherms suggest that the flow pattern is characterized by a weak single cell circulation and heat transfer is mainly through heat conduction for both aspect ratios. The center of the single cell is located at a point closer to the ceiling for these cases. For $a_r = 0.5$, the circulation becomes stronger and center of the cell moves downwards slightly as Rayleigh number increases. For $a_r = 0.25$, on the other hand, the variation of Rayleigh number in low Rayleigh range ($Ra \leqslant 10^5$) does not affect the flow and temperature fields considerably, persisting on a regime similar to that of pure conduction. The cell does not occupy the entire enclosure for this case. At higher Rayleigh numbers, when $Ra \geqslant 10^5$ for $a_r = 0.5$ and when $Ra \geqslant 10^6$ for $a_r = 0.25$, the flow occupies the whole enclosure with the exception of lower left corner at which thermally inactive walls intersect and bottom wall imposes a severe restriction on the flow. With increasing Rayleigh numbers, the isotherms are compressed towards the hot wall and the cold ceiling and most of the enclosure is occupied by warmer fluid. Due to this effect, the single cell is expanded in both vertical and horizontal directions with a slight distortion in flow direction. This expansion results in boundary layer formation at $Ra = 10^6$ for $a_r = 0.5$ and at $Ra = 10^7$ for $a_r = 0.25$. Convection in boundary layers alters the sign of temperature gradients in turn, and thus a secondary cell formation occurs in the core region (Fig. 5(e)).

3.4. Nusselt number for hot vertical wall

Based on numerical temperature data, local and average Nusselt numbers are calculated using eqns (12)–(15). Since we are dealing with a steady state problem with no heat generation and no viscous energy dissipation, it is clear, from the overall energy balance, that the average Nusselt numbers for the heated side wall and the cooled ceiling are not independent of each other. The overall energy balance for the enclosure yields the following relation between these two Nusselt numbers:

$$\overline{Nu_x} = \overline{Nu_y}/a_r \tag{17}$$

Keeping this point in mind, the influence of Rayleigh number and aspect ratio on heat transfer within the enclosure is investigated by considering $\overline{Nu_y}$ as the basic heat transfer parameter. The influence of Rayleigh number on average Nusselt number for heated vertical wall is shown in Fig. 7 for various aspect ratios. At low Rayleigh numbers ($Ra \leqslant 10^4$), especially for tall enclosures ($a_r < 1$), the influence of Rayleigh number on average Nusselt number is not significant. The influence becomes stronger as Rayleigh number increases beyond 10^4. The Nu–Ra relation follows the power law $Nu \sim Ra^{1/4}$ approximately beyond $Ra = 10^4$ for square ($a_r = 1$) and shallow ($a_r > 1$) enclosures, and beyond $Ra = 10^5$ for tall enclosures. The effect of aspect ratio on average Nusselt number is demonstrated in Fig. 8 more clearly. It can be observed from the figure that the influence of aspect ratio on average Nusselt number differs in significance for tall and shallow enclosures. For the case of tall enclosure, the dependence of Nusselt number on aspect ratio is represented by a sharper slope in $Nu-a_r$ curve for a fixed Rayleigh number. The slopes of the curves increase as the aspect ratio decreases implying a stronger aspect ratio effect. For the case of shallow enclosure, on the other hand, the average Nusselt number has a weak dependence on aspect ratio, particularly at low Rayleigh numbers. The insensitiveness of the average Nusselt number on aspect ratio variation for this case can be attributed to the partially inactive section of the cold ceiling when the aspect ratio is large. In the same figure, pure conduction solution is also shown for comparison purposes. The average Nusselt number for pure conduction case is calculated using the closed form expression below, obtained through the use of separation of variables

$$\overline{Nu_y} = \sum_{m=1}^{\infty} \frac{(\sin \beta_m)^2}{\beta_m} \tan h \beta_m a_r \tag{18}$$

where β_ms are the eigenvalues and calculated from

$$\beta_m = (2m-1)\tfrac{\pi}{2} \tag{19}$$

From the figure it is clear that numerical results for $Ra = 10^3$ agree well with the analytical solution exhibiting nearly pure conduction characteristics.

Comparison of present results with those of Refs. [2] and [21] is shown in Fig. 9 At high Rayleigh numbers, $Ra \geqslant 10^6$, there is no discernible difference between the results from the present study and from Refs. [2, 21]. At low Rayleigh numbers, $Ra < 10^5$, on the other hand, average Nusselt numbers obtained in this study are quite higher than those given in [2, 21]. This difference is obviously related to the difference in physical boundary conditions under consideration. In the previous studies, the

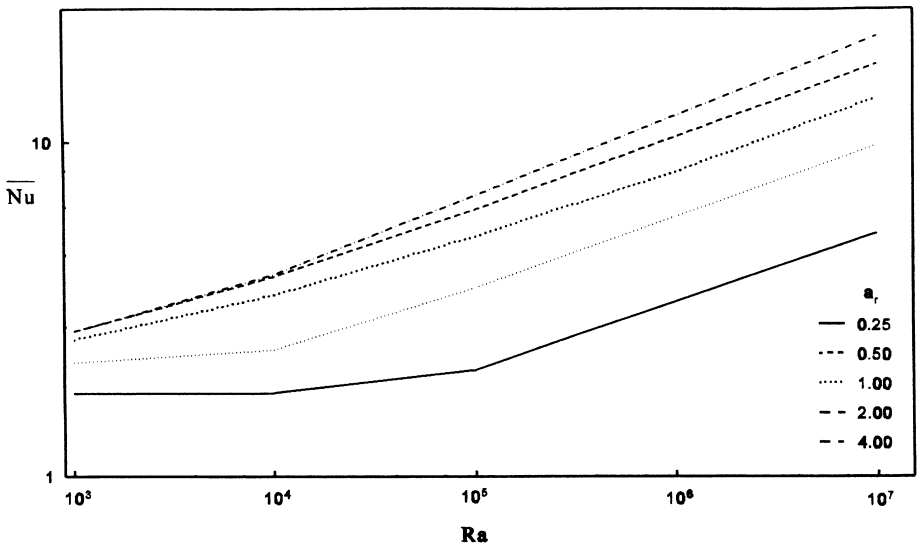

Fig. 7. Variation of average Nusselt number at the heated wall with Rayleigh number.

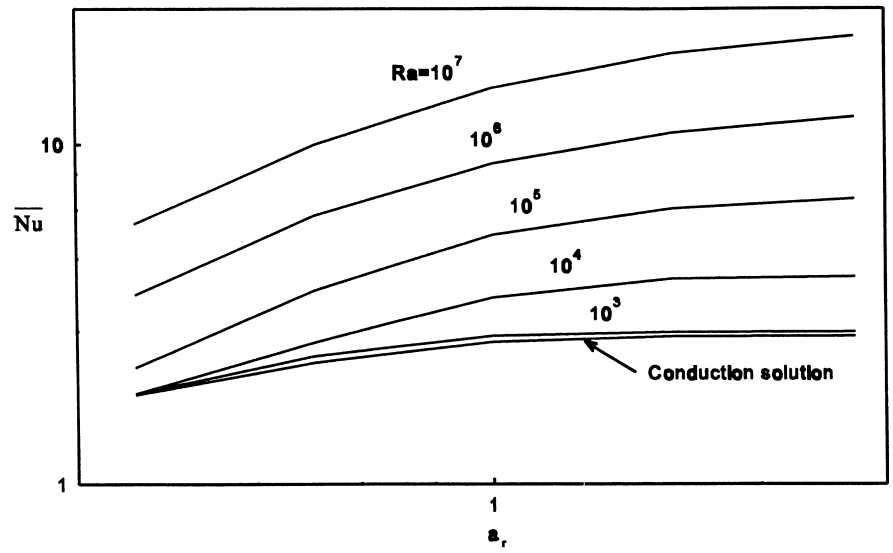

Fig. 8. Variation of average Nusselt number at the heated wall with aspect ratio.

enclosure is heated from one side and cooled from the other side, while heating from one side and cooling from ceiling is considered in this study. In low Rayleigh range, the dominant energy transport mechanism is conduction and it takes shorter distance for heat to diffuse from hot wall to cold ceiling in case of cold ceiling application compared to the case of side cooling, thus resulting in higher Nusselt numbers as it is observed from Fig. 9. In high Rayleigh range a boundary layer is established on the hot wall and the dominating mechanism is convection. A similar single cell forms within the enclosure for both cases carrying the same amount of overall energy from the hot wall to the cold wall. In moderate Rayleigh range, $10^5 \leqslant Ra \leqslant 10^6$, energy transport through diffusion and convection are comparable. Again due to more effective conduction, the cold ceiling system has a better heat transfer efficiency over the cold side wall system.

4. Conclusions

In this study we presented the results of a numerical study of buoyancy-induced flow and heat transfer in a

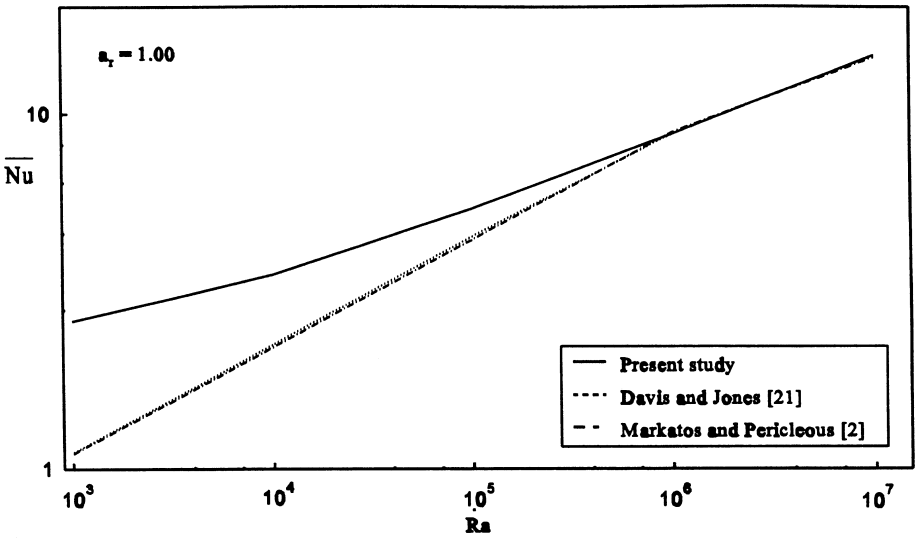

Fig. 9. Comparison of the present results (for a square enclosure with heated side wall and cooled ceiling) with the results (for a square enclosure with heated and cooled side walls) of Davis and Jones [21] and Markatos and Pericleous [2].

two-dimensional enclosure isothermally heated from one side and cooled from the ceiling. The influence of Rayleigh number on fluid flow and heat transfer is investigated in the range of $10^3 \leqslant Ra \leqslant 10^7$. Regarding the effect of enclosure configuration, four different aspect ratios $a_r = 0.25$, 0.5, 2.0, and 4.0 are considered besides square enclosure ($a_r = 1$). For each aspect ratio it is found that a clockwise rotating single cell exists for $Ra \leqslant 10^6$. For $Ra = 10^7$, a secondary cell is observed for all cases except for $a_r = 0.25$. For the case of tall enclosure ($a_r < 1$), average Nusselt number does not change significantly in low Rayleigh range ($Ra \leqslant 10^4$) while it has a rather strong dependence on Rayleigh number in high Rayleigh range ($Ra \geqslant 10^5$) and the warmer fluid occupies nearly the entire enclosure. For square and shallow enclosures ($a_r \geqslant 1$), average Nusselt number increases monotonically with increasing Rayleigh number and a major part of the enclosure is occupied by colder fluid especially at high Rayleigh numbers. Compared to the results of previous studies in which partially heated square enclosures are considered, present heat transfer results are found to be superior especially in conduction dominated low Rayleigh regions.

References

[1] S. Ostrach, Natural convection in enclosures. Journal of Heat Transfer 110 (1988) 1175–1190.
[2] N.C. Markatos, K.A. Pericleous, Laminar and turbulent natural convection in an enclosed cavity. International Journal of Heat and Mass Transfer 27 (1984) 755–772.
[3] K. Kübleck, G.P. Merker, J. Straub, Advanced numerical computation of two-dimensional time-dependent free convection in cavities. International Journal of Heat and Mass Transfer 23 (1980) 203–217.
[4] Z.Y. Zhong, K.T. Yang, J.R. Lloyd, Variable property effects in laminar natural convection in a square enclosure. Journal of Heat Transfer 107 (1985) 133–138.
[5] L.-G. Sundström, S. Kimura, On laminar free convection in inclined rectangular enclosures. Journal of Fluid Mechanics 313 (1996) 343–366.
[6] P. Filis, D. Poulikakos, An experimental study of the effect of wall temperature non-uniformity on natural convection in an enclosure heated from the side. International Journal of Heat and Fluid Flow 7 (1986) 258–265.
[7] T.-H. Hsu, C.-K. Chen, Natural convection of micropolar fluids in a rectangular enclosure. International Journal of Engineering Science 34 (1996) 407–415.
[8] S.M. Elsherbiny, Free convection in inclined air layers heated from above. International Journal of Heat and Mass Transfer 39 (1996) 3925–3930.
[9] M. Hasnaoui, E. Bilgen, P. Vasseur, Natural convection heat transfer in rectangular cavities heated from below. Journal of Thermophysics and Heat Transfer 6 (1992) 255–264.
[10] M.M. Ganzarolli, L.F. Milanez, Natural convection in rectangular enclosures heated from below and symmetrically cooled from the sides. International Journal of Heat and Mass Transfer 38 (1995) 1063–1073.
[11] A. Valencia, R.L. Frederick, Heat transfer in square cavities with partially active vertical walls. International Journal of Heat and Mass Transfer 32 (1989) 1567–1574.
[12] R.B. Chinnokotla, D. Angirasa, R.L. Mahajan, Parametric study of buoyancy-induced flow and heat transfer from L-shaped corners with asymmetrically heated surfaces. International Journal of Heat and Mass Transfer 39 (1996) 851–865.
[13] E.E. Selamet, V.S. Arpaci, C. Borgnakke, Simulation of

laminar buoyancy-driven flows in an enclosure. Numerical Heat Transfer 22 (1992) 401–420.
[14] H.H.-S. Chu, S.W. Churchill, C.V.S. Patterson, The effect of heater size, location, aspect ratio, and boundary conditions on two-dimensional, laminar, natural convection in channels. Journal of Heat Transfer 98 (1976) 1194–1201.
[15] M. November, M.W. Nansteel, Natural convection in rectangular enclosures heated from below and cooled along one side. International Journal of Heat and Mass Transfer 30 (1987) 2433–2440.
[16] D. Poulikakos, Natural convection in a confined fluid-filled space driven by a single vertical wall with warm and cold regions. Journal of Heat Transfer 107 (1985) 867–876.
[17] O. Aydin, A. Ünal, T. Ayhan, Numerical solutions for buoyancy-driven flow in a 2-D square enclosure heated from one side and cooled from above. Proceedings of the Advances in Computational Heat Transfer Symposium, Begell House, New York, 1997, pp 387–394.
[18] D. Elkaim, M. Reggio, R. Camarero, Simulating two-dimensional turbulent flow by using the k–ε model and the vorticity-stream function formulation. International Journal of Numerical Methods in Fluids 14 (1992) 961–980.
[19] P.J. Roache, Computational Fluid Dynamics, Hermosa, Albuquerque, NM, 1982, p. 91.
[20] S.V. Patankar, Numerical Heat Transfer and Fluid Flow, Hemisphere, Washington, 1980, p. 67.
[21] G. de Vahl Davis, J.P. Jones, Natural convection in a square cavity, a comparison exercise. International Journal of Numerical Methods in Fluids 13 (1983) 227–248.